

Journal of Materials Chemistry A

Accepted Manuscript



This is an *Accepted Manuscript*, which has been through the Royal Society of Chemistry peer review process and has been accepted for publication.

Accepted Manuscripts are published online shortly after acceptance, before technical editing, formatting and proof reading. Using this free service, authors can make their results available to the community, in citable form, before we publish the edited article. We will replace this *Accepted Manuscript* with the edited and formatted *Advance Article* as soon as it is available.

You can find more information about *Accepted Manuscripts* in the [Information for Authors](#).

Please note that technical editing may introduce minor changes to the text and/or graphics, which may alter content. The journal's standard [Terms & Conditions](#) and the [Ethical guidelines](#) still apply. In no event shall the Royal Society of Chemistry be held responsible for any errors or omissions in this *Accepted Manuscript* or any consequences arising from the use of any information it contains.

Biomimetic snowflake-shaped magnetic micro-/nanostructures for highly-efficient adsorption of heavy metal ions and organic pollutants from aqueous solution

Xiaoman Zhang,^{ab} Jinyun Liu,^{*ac} Sean Joseph Kelly,^c Xingjiu Huang^a and Jinhui Liu^{*a}

^a Research Center for Biomimetic Functional Materials and Sensing Devices, Institute of Intelligent Machines, Chinese Academy of Sciences, Hefei 230031, PR China

^b Department of Chemistry, University of Science and Technology of China, Hefei 230026, PR China

^c Frederick Seitz Materials Research Laboratory, Beckman Institute for Advanced Science and Technology, University of Illinois at Urbana-Champaign, Urbana, IL 61801, USA

* Address correspondence to J. Y. Liu and J.H. Liu

E-mail: jyliu@illinois.edu (J.Y. Liu), jhliu@iim.ac.cn (J.H. Liu)

Tel.: +01 217 721 2414

Abstract: Some conventional micro- or nano-structured adsorbents are subjected to the issue that they can hardly show most of their adsorbing sites for adsorbing pollutants in solution because of serious aggregation of adsorbents. Here, we present a biomimetic strategy for designing novel adsorbents which can promisingly address this issue. The prepared ZnO@SiO₂@Fe₃O₄/C micro-/nanostructures have a special snowflake-shaped morphology, which enables them to keep a relatively large space remaining between connected adsorbents, and thereby reduce the overlap and coverage of the adsorbing sites. The adsorbents also possess porous and multi-layered structures, which are advantageous to achieve a large surface area for adsorption. The magnetic Fe₃O₄/C coating ensures this adsorbent can be easily collected from solution and recycled for subsequent uses. In adsorbing measurements, Pb(II) and As(V) were employed as heavy metal ions, while methylene blue was used as an organic probe. The kinetic adsorption process, maximum adsorption capacity, and pH-dependent adsorbing effect were investigated systematically. We find that the kinetic process and isotherm can be fitted with a pseudo-second-order model and Langmuir adsorption model, respectively. The adsorbing performance of the snowflake-shaped adsorbents has been compared with that of a spherical adsorbent. The mechanism has been demonstrated from the special biomimetic structure. In addition, the recycling performance based on magnetic collection and basic desorption has also been investigated.

Keywords: bio-inspired structure; heavy metal ions; adsorption; removal efficiency

1. Introduction

Removal of pollutants from water has received extensive attention due to its significance in the protection of human health and maintenance of biological environments.¹⁻⁵ Heavy metal ions such as Pd(II), Cd(II), As(V) and Cr(VI), which are mainly released from industrial production and dissolved from natural minerals, can be acutely harmful to our health.^{6,7} Further, organic pollutants such as industrial dyes released from printing processes are serious risk factors for conditions including cancer and skin diseases. As a result, a process to remove them from water is highly desired. In recent years, among various purification methods, an adsorption approach has been of great interest because of its low-cost, easy construction and operation, and so on. Many efforts have been made to develop novel adsorbents with the aim of high efficiency and good recyclability.⁸⁻¹⁰ Recently, nanostructured adsorbents have been considered a promising candidate because of their large surface area, high surface activity, easy of modification with more specifically functional groups, etc.¹¹⁻¹³ However, the small size of nanostructured adsorbents increases the likelihood of heavy aggregation during the adsorption process. Numerous adsorption sites of materials are covered making interaction with pollutants like heavy metal ions or organic molecules in water difficult, thereby greatly reducing the adsorption efficiency.¹⁴⁻¹⁶ In this condition the potential benefits of nanostructures are hardly utilized. Thus, there remains the challenge of making these advantages of nanostructures effective for adsorbing pollutants.

As we know, the natural world contains a variety of amazing structures that possess specific characters, many of which have been found to be valuable for human design.¹⁷⁻¹⁹ In our previous investigations,²⁰⁻²² we found that some leaf-shaped and coral-like micro-/nanostructures exhibited significantly enhanced performance for diffusion and adsorption compared to conventional

structures. The structural advantages of these bio-inspired structures enable them to be promisingly applied for design efficient dye-sensitized solar cells and more sensitive sensors. Here, we know that snowflakes possess a special morphology that promotes excellent dispersion while naturally falling from the sky. The sharp angles of snowflakes allow them to keep a relatively large space even though they may contact each other. Inspired by this point, we proposed that the snowflake-shaped structure can be applied to address the aggregation of nanoadsorbents during adsorption of pollutants which overlaps many adsorption sites. The remained space formed by the special snowflake-shaped structure can be employed to improve the adsorption efficiency. Moreover, on the basis of the snowflake-shaped structure, we can also perform additional functionalizations to further improve the adsorption performance.

Here, we present a biomimetic concept to design novel adsorbents for efficient adsorption of pollutants from aqueous solution. As illustrated in Scheme 1, a snowflake-shaped ZnO micro-/nanosstructure, which simultaneously possesses a porous structure, was prepared through a facile hydrothermal route followed by a sintering process. It was used as a template for further functionalization. Next, the snowflake-shaped ZnO was coated with a SiO₂ layer in order to solvothermally grow a magnetic Fe₃O₄/carbon composite coating. By doing so, we finally obtain a snowflake-shaped magnetic ZnO@SiO₂@Fe₃O₄/C structure, which possesses the following features: 1) the special snowflake-shaped morphology significantly reduces the overlap of adsorption sites due to aggregation; 2) the pores throughout the flakes enable the structure to exhibit a large surface area, which is advantageous for both Fe₃O₄ growth and pollutant adsorption; 3) magnetic Fe₃O₄ coating provides substantial recyclability for this adsorbent, which can reduce the cost and simplify potential usage. In our investigation, the adsorbing properties towards heavy metal ions (including

Pb(II) and As(V)) and organic pollutants (methylene blue was used as a probe) were examined systematically; these include kinetic adsorption processes, adsorption capacity, pH-dependent effect, adsorption behavior fitted by Langmuir model, recyclability, as well as the performance comparison with spherical structures.

2. Experimental section

2.1 Preparation of the snowflake-shaped precursors and porous ZnO micro-/nanostructures

All chemicals were analytical grade and used without further purification as purchased from Shanghai Chemical Reagents Company. The preparation of the snowflake-shaped precursors was similar to the previous report with some modifications.²³ In a typical procedure, 0.002 mol of $\text{Zn}(\text{NO}_3)_2$ and 0.01 mol of urea were dissolved into 60 mL of de-ionized water under constant stirring for 2 h to form a homogeneous solution. Then, the solution was transferred into a Teflon-lined stainless steel autoclave (HR-80 model, Wuxi Bojue Chemical Equipment Company). The autoclave was sealed and heated in a program-controlled oven at 130 °C for 3 h. After being cooled to room temperature naturally, the precipitates were collected via centrifuge (TG-18G model, Kait Experimental Instrument Company) and washed several times with de-ionized water and ethanol alternately. The obtained samples were dried in an oven at 60 °C for 4 h. In order to get the porous ZnO micro-/nanostructures, the samples were further sintered in a tube furnace at 500 °C for 1.5 h in air. The elevating rate of the temperature was 10 °C min⁻¹.

2.2 Coating of the ZnO with a SiO₂ layer

The snowflake-shaped porous ZnO micro-/nanostructures were coated with a SiO₂ layer via the

Stober method. Typically, 8 mL of de-ionized water and 1.5 mL of ammonium hydroxide were mixed with 40 mL of ethanol. 0.03 g of the prepared ZnO micro-/nanostructures was dispersed in the solution under ultrasonication for 10 min. Subsequently, 0.5 mL of tetraethylorthosilicate (TEOS) was added into the solution drop by drop under constant stirring. After stirring for 2 h, the samples were collected via centrifuge and washed for 3 times with de-ionized water and ethanol alternately. At last, the obtained samples were dried in an oven at 60 °C for 3 h.

2.3 Growth of magnetic Fe₃O₄/C composite onto the ZnO@SiO₂ micro-/nanostructures

The Fe₃O₄/C composite layer was grown onto ZnO@SiO₂ via a solvothermal approach. 0.2 g of ferrocene was dissolved into 60 mL of acetone to form a homogeneous solution. 0.05 g of ZnO@SiO₂ was dispersed in the solution under stirring for 10 min. Then, 2.0 mL of hydrogen peroxide (30 wt.%) was added into the solution under ultrasonication for 30 min. After that, it was transferred into a Teflon-lined steel autoclave with a capacity of 80 mL. The sealed autoclave was heated at 195 °C for 24 hours. As the autoclave was cooled down to room temperature naturally, the precipitates were collected and washed with ethanol and de-ionized water. The obtained samples were dried in a vacuum oven at 60 °C, and kept for further use.

2.4 Characterizations

The samples were characterized by using a Philips X' Pert Pro X-ray diffractometer (XRD) with Cu K α radiation (1.5418 Å), a FEI Sirion 200 field emission scanning electronic microscope (FESEM), and a JEOL JEM-2010 transmission electron microscope (TEM) equipped with an Oxford INCA energy dispersive x-ray analyser (EDX) at an accelerating voltage of 200 kV. The

elemental mappings and the line scans were carried out in the high-angle annular dark-field mode on the same TEM. The XRD peaks of the crystalline phases were compared with the patterns in the Joint Committee on Powder Diffraction Standards (JCPDS). Elements and state analysis was performed on an ESCALab MK II X-ray photoelectron spectrometer (XPS) using non-monochromatized Mg K α X-ray beams as the excitation source. Binding energies were calibrated relative to the C1s peak at 284.6 eV. The specific surface area was measured on a Coulter Omnisorp 100CX Brunauer–Emmett–Teller (BET) instrument by using N₂ adsorption and desorption. A Fourier transform infrared (FTIR) absorption spectrum was recorded by a Shimadzu IR-440 spectrometer from 4000 to 500 cm⁻¹.

2.5 Adsorption measurements

The adsorption experiments were carried out in a vibration water bath at a constant temperature of 25 °C. Both heavy metal ions and organic pollutant were employed as pollutants in water for adsorption measurements. As for the adsorption of heavy metal ions, 20 mL of Pb(II) or As(V) aqueous solutions (pH value was 7) with different initial concentrations (ranging from 2 to 200 ppm for isothermal curves measurements; 20 ppm for kinetic process investigations) were dispersed with 25 mg of the as-prepared adsorbents. After a certain period of adsorbing time, the remaining solutions were separated and collected by using magnet to remove adsorbents. The remaining concentration of the heavy metal ions was measured by a Jarrell-Ash ICAP-9000 model inductively coupled plasma (ICP). For the investigation of pH value dependent effect, a series of Pb(II) or As(V) aqueous solutions at a pH value from 3 to 10 were adjusted by HCl and NaOH solutions. Typically, after adding a certain amount of acid or base solution, a small volume of solution was transferred

and measured by a pH meter (Fisher Science Education). This procedure proceeded until the solution was adjusted to the aided pH value. After that, the adsorption procedures were carried out. The initial concentrations of Pb(II) and As(V) were 5 ppm, and the adsorption time was 3 h. As for the recycle adsorption study, Pb(II) solutions were taken as an example. The procedures were as follows: 25 mg of adsorbents were dispersed into a 5 ppm Pb(II) solution (pH value was 7); adsorption for 3 h in a vibration water bath; separating adsorbents from solution by a magnet; dispersing adsorbents into basic solution (pH value is 10) under mechanical stirring; collecting adsorbents by magnet; washing with de-ionized water and drying at 60 °C for 4 h for next use. During each cycle, the remaining concentration of the Pb(II) solution after removal of adsorbents was measured by ICP for efficiency calculation.

For the adsorption of organic pollutant, methylene blue (MB) was employed as the probe for measurements. Typically, in an isothermal adsorption measurement, 20 mg of the adsorbents were dispersed into 20 mL of MB aqueous solution (in a centrifuge tube) by ultrasonication for 1 min. The tube was left for 3 h in a vibration water bath. After that, the adsorbents were separated from the solution by magnet. A UV-Vis spectrophotometer (CARY-5E) was used to determine the remaining concentration of MB solution by standard spectrophotometric methods with $\lambda = 664$ nm. The initial concentration of MB solutions for isothermal adsorption measurements was ranged from 2 to 200 ppm. In the kinetic process study, the MB solutions at an initial concentration of 40 ppm were used; while in the pH value dependent effect investigation, the procedures were the same as the ones for heavy metal ions.

3. Results and discussion

3.1 Morphology, structure and composition of the adsorbents

Fig. 1 shows a series of samples prepared during the procedure. As can be seen from Fig. 1a, the synthesized precursor exhibits a special snowflake-shaped morphology. It is composed of hexagonal flakes in a size of about 10 μm . Seen from the profile-view (Supporting Information Fig. S1a† and b†) and high-magnification SEM images (Fig. S1c†), it can be found that it shows a multi-layered structure. A large amount of layers assemble together layer by layer. The thickness of each layer is about 20 to 30 nm. As we know, layered structures have been of great interest for developing novel adsorbents. Many reports have demonstrated that such structures can provide layered surface areas, thereby giving a good adsorption performance. Here, the multi-layered precursors would also give promise for further preparing novel adsorbents which possess excellent adsorption capability. The composition of the precursors can be confirmed as $\text{Zn}_4(\text{CO}_3)(\text{OH})_6 \cdot \text{H}_2\text{O}$ by the XRD pattern compared to the literature (JCPDS Card No. 11–0287), as shown in Fig. 1h.

After a sintering treatment in air, the precursors were converted to porous ZnO, as shown in Fig. 1b. The snowflake-shaped structure keeps well without damage, and we find that there are numerous pores formed throughout the entire structure which can be ascribed to the decomposition of organic and hydrate composites in the precursor, as well as a secondary re-crystallization process.^{24,25} This pore size is about 60 to 80 nm, displayed specifically in the high-magnification SEM image (Fig. 1c) and further supported by the BET measurement which will be shown below. By using this porous ZnO micro/nanostructure as template, a SiO_2 coating process was carried out. As observed in Fig. 1d and e, the coating layer is clearly present. The thickness of the SiO_2 coating is about 20 nm. It should be noted that the thickness of the SiO_2 coating cannot be too thick or thin. In our study, as the pore size ranges from 60 to 80 nm, thick coatings (around 30 to 40 nm) will

block the pores; while thin coatings (smaller than 10 nm) can hardly grow with Fe_3O_4 layer further. We find that the amount of TEOS used for coating obviously influences the thickness, as shown in Fig. S2†. In our study, 0.5 mL of TEOS achieved an ideal coating for further fabrication.

Fig. 1f and g show the final products prepared by solvothermally growing a $\text{Fe}_3\text{O}_4/\text{C}$ composite onto the snowflake-shaped $\text{ZnO}@/\text{SiO}_2$. These still show an excellent snowflake-shaped morphology, as well as a multi-layered porous structure. From the high-magnification SEM image (Fig. 1g), an extra rough layer can be observed on the surface. In addition, the pore remains in a reduced size of ca. 30 nm. In its XRD pattern (Fig. 1h), the diffraction peaks at ca. 30.4° , 35.5° , and 43.6° can be indexed to the (220), (311), and (400) crystalline planes of Fe_3O_4 , respectively. It is in good agreement with the reference of JCPD Card (No: 98-0294), further confirming the growth of Fe_3O_4 .

The formation of $\text{Fe}_3\text{O}_4/\text{C}$ composite is first demonstrated from TEM observations, as shown in Fig. 2. From Fig. 2a, we can see the snowflake-shaped morphology which is consistent with the previous SEM observations. Besides, similar morphologies from the SiO_2 -coated and pure ZnO can also be confirmed by TEM images (Fig. S3†). The layer-by-layer structure is presented in Fig. 2b and c. As marked in Fig. 2c, we can see the SiO_2 layer coats on ZnO core, while a Fe_3O_4 and carbon composite layer grows on the SiO_2 coating. Moreover, we find that the $\text{Fe}_3\text{O}_4/\text{C}$ composite is porous rather than a compacted film. This is advantageous to achieve a large surface area and provide numerous sites for adsorption of pollutants. From the XPS analysis (Fig. 2d), it can be found the samples are composed of Zn, Si, and Fe. The carbon and oxygen peaks, besides coming from the samples, can also be attributed to the adsorbed CO_2 , H_2O , or the small organic molecules during measurements. However, in our case accompanying with the XRD and TEM results, it is reasonable

to believe that most of them should come from the prepared samples.

The composition of the prepared micro-/nanostructure was further investigated using elemental mappings, as shown in Fig. 3. We can see that the Si and Fe distribute densely throughout the entire structure. The Zn element locates at the core position in a smaller size compared with the else two elements. The uniform distribution of Si and Fe also indicate that the coatings of SiO₂ and Fe₃O₄, respectively, are uniform. Additionally, we carried out an EDX analysis (Table S1†), which shows that the molar ratio of Zn: Si: Fe is about 2.88: 8.35: 3.54.

We know that surface area and functional groups on the surface are two significant factors for influencing the adsorbing capability of adsorbents.^{26–28} In our investigation, on one hand, we measured the surface area of the prepared snowflake-shaped micro-/nanostructures, as shown in Fig. 4. From Fig. 4a, we can see that it exhibits a type-IV isotherm with a hysteresis loop from ca. 0.5 to 1.0 (P/P₀).^{29,30} The value of BET surface area is found to be about 79.2 m² g⁻¹. Moreover, the pore-size distribution was also measured by using the Barrett–Joyner–Halenda (BJH) method, as shown in Fig. 4b. Interestingly, it can be found that there are two dominating pore diameters of about 4 and 50 nm. On the basis of the SEM and TEM observations, the pore-size of ca. 50 nm can be ascribed to the pores throughout the flakes originally formed by the porous ZnO. The smaller one (4 nm) is more likely formed among the Fe₃O₄/C composites, since we noted that they are structurally loose instead of a tight film. Furthermore, in order to investigate the functional groups on the surface of the prepared adsorbents, FTIR spectrum was also recorded, as shown in Fig. 5. The peaks at ca. 2870 and 1410 cm⁻¹ can be assigned to the stretching and bending vibrations of C–H,³¹ respectively. It indicated there are some organic components in the prepared samples, which is consistent with the analysis on the existence of carbon composite demonstrated above. The strong

and broad –OH peak located from 3100 to 3600 cm^{-1} is most likely due to the chemical bonds on the surface of adsorbents and the adsorbed water in the sample. The mechanism of the formation of organic component in the final product can be explained from the following aspect: during solvothermal growth, ferrocene, which was used as the source of iron, was decomposed. In this condition, amorphous carbon and some organic components can be produced together with Fe_3O_4 . Therefore, by combining with the BET and FTIR investigations, we can see that the prepared adsorbents possess a large surface area, porosity, and some organic components with functional groups. This is promising to achieve a good adsorbing performance. For example, the negative hydroxyl groups can exhibit high adsorbing capacity towards positive metal ions (such as Pb(II) in our study) and organic pollutants.

3.2 Adsorbing properties towards heavy metal ions and organic pollutant

3.2.1 Kinetic adsorption process

In order to investigate the adsorbing performance of the prepared biomimetic structured adsorbents, Pb(II) and As(V) were employed as heavy metal ions for adsorption; while MB was used as an organic pollutant probe. Fig. 6 shows the kinetic processes of the adsorbents towards different targets. As can be seen from Fig. 6a, the efficiencies increase rapidly at the initial period for all of targets. For Pb(II) and MB, the removal efficiencies can be about 32% and 46% respectively after an adsorption time of less than 3 min, indicating an excellent adsorbing rate of the prepared $\text{ZnO@SiO}_2@\text{Fe}_3\text{O}_4/\text{C}$ adsorbents. Compared with some other reports, this performance shows promising improvement. For example, it was reported that an activated carbon with high mesoporosity and abundant oxygen-containing functional groups showed a removal efficiency of

about 23.3% after 10 min contact (condition: 1.0 g L⁻¹ adsorbents put into Pb(II) solution with initial concentration of 150 mg L⁻¹).³² In addition, a Fe_{0.01}Ni_{0.01}Zn_{0.98}O/polyacrylamide nanocomposites was found to exhibit adsorption efficiency of about 5.71% in 30 min towards MB with an initial concentration of 10 ppm.³³

As compared with As(V) which is as the form of H₂AsO₄⁻ and HAsO₄²⁻ in water especially in under the pH value from 4 to 10,³⁴ Pb(II) is positive as ions. The negative groups on the surface of the as-prepared samples can be more likely adsorbing positive ions compared with negative ones, which could be the potential reason for the different efficiencies for Pb(II) and As(V). Similarly, MB is also a typical positive dye, which can be easily adsorbed onto the adsorbents by electrostatic force. Furthermore, we find that the kinetic processes can be fitted well by a pseudo-second order model, as shown in Fig. 6b. The pseudo-second-order model can be presented as Equation (1).³⁵⁻³⁷

$$\frac{dq_t}{dt} = k_2(q_e - q_t)^2 \quad (1)$$

$$y = 0.03656x + 1.0142 \quad R^2 = 0.9985 \quad (2)$$

$$y = 0.1517x + 20.0285 \quad R^2 = 0.9539 \quad (3)$$

$$y = 0.02245x + 0.4192 \quad R^2 = 0.9916 \quad (4)$$

where k_2 is the rate constant. In this model, it assumes that the difference between the concentration (q_t) at time t and the saturated adsorption amount (q_e), is the driving force for the adsorption. The fitted results can be expressed as Equations (2) to (4), which stand for the adsorption towards Pb(II), As(V), and MB, respectively.

3.2.2 Maximum adsorption capacity

Since the capacity of an adsorbent is very important for potential applications, a series of

isothermal adsorptions were investigated, as shown in Fig. 7. From Fig. 7a, we can see that the adsorption turns out to be saturated depending on the increase of concentration. The maximum adsorption capacities of the snowflake-shaped ZnO@SiO₂@Fe₃O₄/C micro-/nanostructures are found to be 94.3, 23.6, and 142.9 mg g⁻¹ towards Pb(II), As(V), and MB, respectively. In addition, the profile of each isotherm is typical Langmuir adsorption, as can be presented in Equation (5).³⁸⁻⁴⁰ In this equation, C_e is the equilibrium concentration of solution (mg L⁻¹), q_e is the equilibrium capacity of the adsorbents (mg g⁻¹), q_m stands for the maximum adsorption capacity, and K_L is the Langmuir adsorption constant (m² mg⁻¹). In the Langmuir isothermal model, it is assumed that there is monolayer coverage of the adsorption surface and no subsequent interaction among adsorbed molecules. By following this model we fitted the isothermal data, as shown in Fig. 7b. It can be found that each line matches well with the Langmuir model. The fitting results are shown in Equations (6) to (8) which stand for the adsorption towards Pb(II), As(V), and MB, respectively. The adsorbing capacity of the biomimetic snowflake-shaped adsorbents is competitive compared with some other reports, as well as active carbon.⁴¹⁻⁴⁴

$$\frac{C_e}{q_e} = \frac{1}{q_m K_L} + \frac{C_e}{q_m} \quad (5)$$

$$y = 0.0106x + 0.0814 \quad R^2 = 0.9864 \quad (6)$$

$$y = 0.0424x + 0.0033 \quad R^2 = 0.9616 \quad (7)$$

$$y = 0.0070x + 0.1020 \quad R^2 = 0.9775 \quad (8)$$

Furthermore, we prepared some magnetic microspheres via similar procedures with microspheres as growth templates, and also investigated their adsorbing properties for comparison. The morphology and structure of the microspheres are shown in Fig. S4†. They also exhibit multi-layered structure. The size of each entire sphere is about 5 to 8 μm; while the thickness of the

layers is around 30 nm. In addition, it should be noted that the pores throughout the layers could hardly be found because of the relatively small and tight sheet-shaped structure. The adsorption conditions for the microspheres are the same as the ones for the snowflake-shaped micro-/nanostructures. After adsorbing measurements, we find that the maximum adsorption capacities of the microspheres towards Pb(II), As(V) and MB are about 54.6, 17.2, and 82.0 mg g⁻¹, respectively, as shown in Fig. S5a and b†. They are obviously smaller than that of the snowflake-shaped adsorbents (Fig. S5c†). The potential mechanism can be explained as follows: this can be attributed to the improved dispersion of the snowflake-shaped structure. The special biomimetic structure can keep a relatively large remaining space between connected adsorbents, which can still give a large effective surface for adsorption. The microspheres aggregate heavily in solution, which makes it hard to show the covered adsorbing sites to targets effectively. Of course, the reduced porosity of the microspheres would also be a part of the potential reason, which is valuable for further investigations. In addition, we compare the adsorption properties of the snowflake-shaped adsorbents with some other reports (Table 1), the presented adsorbents also show improved performance, which makes them promising for potential applications.

3.2.3 pH-dependent effect and recycling performance

The pH-dependent effect is valuable for both achieving maximal adsorbing efficiency and desorbing treatments for reuse. Here, we also investigated the adsorbing properties of the snowflake-shaped ZnO@SiO₂@Fe₃O₄/C micro-/nanostructures under different pH values, as shown in Fig. 8a. In our measurements, the initial concentrations of Pb(II), As(V), and MB were 5 ppm, and the adsorbing time was 3 h. As we know, ZnO can be dissolved under both acidic and basic

surroundings. However, we find that in this condition with low concentration of acid or base, the dissolution of ZnO is tiny. The SiO₂ and Fe₃O₄/C coatings can also be significant protection layers to reduce the dissolution of ZnO. From Fig. 8a, we can see that the adsorbents show stable performance to Pb(II) and MB under acidic condition.

When the solution turns into basic, the adsorbing efficiencies for all the targets decrease, indicating that the prepared adsorbents could be more likely applied for purifying acidic solutions, as well as neutral solutions like drinking water. It should be noted that this is not similar to some other reports about the pH effect. For example, Zhang et al. indicated that the pH regulated the ionization of both Fe₃O₄/C nanoparticles and MB, and thereby influencing the electrostatic interaction and adsorption process.⁵³ Wu et al. proposed that the pH-dependent adsorption should be associated with the functional groups on Fe₃O₄@C nanoparticles and the MB molecules, and the Fe₃O₄@C nanoparticles could be regenerated at low pH values.⁵⁴ In our study, the relatively low adsorption efficiency in the high pH value solutions could be potentially explained by the formation of exceeded hydroxy in basic solution. As we can see from the FTIR spectrum, there are many hydroxy groups (probably from both of the adsorbed water and the adsorbents prepared by multiple steps of solution-based fabrications) on the surface of adsorbents. When the pH value is high (e.g., 10), the hydroxy in solution competitively adsorb positive metal ions and MB molecules (a positive type of dye) instead of improve the adsorption of adsorbents. In contrast, under acid and neutral surroundings, the high density of negative charges on the surface of adsorbents can make it tends to be in a balance, which shows dominate adsorbing force towards positive ions and dyes onto the surface of adsorbents. Of course, the detailed mechanism for such pH value dependent behavior still not clear, which is valuable for further investigations. However, it can be inspired that the desorbing

treatments can be available under basic surroundings.

By following this and taking Pb(II) as an example, the adsorbents were used for adsorption and desorption for three cycles (Fig. 8b). It should be noted that each cycle contains the following steps (as illustrated in Fig. S6[†]): dispersing adsorbents into of Pb(II) solution; adsorbing for 3 h; removing adsorbents by magnet; dispersing adsorbents into basic solution under mechanical stirring; collecting adsorbents by magnet; drying for next use. From Fig. 8b, we can see that the snowflake-shaped ZnO@SiO₂@Fe₃O₄/C micro-/nanostructures exhibit a stable adsorbing efficiency during different cycles, indicating that the prepared adsorbents possess a good recycling capacity.

4. Conclusions

In summary, we present a biomimetic strategy to design novel adsorbents for removal of pollutants from aqueous solution. The prepared snowflake-shaped structure can effectively address the aggregation and overlap issues of conventional micro- or nanoscale adsorbents, and thereby improves the utilization of adsorbing sites. We find that the snowflake-shaped ZnO@SiO₂@Fe₃O₄/C micro-/nanostructures show a high adsorbing efficiency for removing heavy metal ions (Pb(II) and As(V)) and organic pollutant (MB). Especially, the removal efficiencies towards Pb(II) and MB can be about 32% and 46% respectively after a short adsorption time of less than 3 min. The maximum adsorption capacities of the adsorbents towards Pb(II), As(V), and MB are 94.3, 23.6, and 142.9 mg g⁻¹, respectively, significantly higher than the spherical adsorbents. The mechanism for the enhancement is demonstrated from the special biomimetic structure. We also find the kinetic adsorption processes fit the pseudo-second-order model, and the isotherms fit the Langmuir model. In addition, the prepared ZnO@SiO₂@Fe₃O₄/C micro-/nanostructures also

possess good recycling capability. These performances enable the prepared biomimetic adsorbents to be applied for removal of pollutants from aqueous solutions with low-cost, as well as high efficiency and stability. Furthermore, our investigation also demonstrates that the biomimetic strategy can be a promising method for designing novel adsorbents to address the issues of some conventional adsorbents.

Acknowledgments

This work was financially supported by the State Key Project of Fundamental Research for Nanoscience and Nanotechnology (2011CB933700), the National Natural Science Foundation of China (51002157, 21277146, 61071054, 21177131, and 61104205), and the One Hundred Person Project of the Chinese Academy of Sciences. In addition, Prof. Zhaoqin Chu from the Institute of Solid State Physics of Chinese Academy of Sciences was appreciated for her helpful analysis and discussion on elemental mappings. Prof. Xinyao Yu from the Institute of Intelligent Machines of Chinese Academy of Sciences was also appreciated for his help and analysis on the adsorption model fits.

Figure captions

Scheme 1 The illustration for the fabrication of a snowflake-shaped magnetic adsorbent.

Fig. 1 FESEM images of (a) the prepared precursors; (b) and (c) ZnO; (d) and (e) SiO₂-coated ZnO; (f) and (g) ZnO@SiO₂@Fe₃O₄/C micro-/nanostructures; and (h) XRD patterns of the samples.

Fig. 2 TEM images of a single snowflake-shaped ZnO@SiO₂@Fe₃O₄/C; (b) and (c) high-magnification TEM images; and (d) XPS spectrum of the ZnO@SiO₂@Fe₃O₄/C micro-/nanostructures.

Fig. 3 High-magnification TEM image of a part of the snowflake-shaped ZnO@SiO₂@Fe₃O₄/C micro-/nanostructure; elemental mappings of (b) Zn K α , (c) Si K α , and (d) Fe K α .

Fig. 4 (a) Typical N₂ adsorption/desorption isotherm and (b) pore-size distribution curve of the porous ZnO@SiO₂@Fe₃O₄/C micro-/nanostructure.

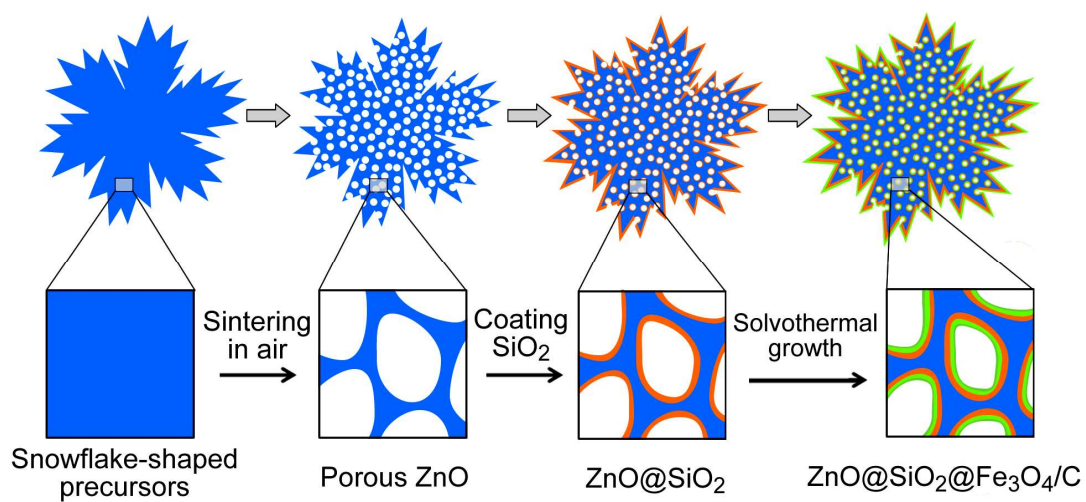
Fig. 5 FTIR spectrum of the snowflake-shaped ZnO@SiO₂@Fe₃O₄/C micro-/nanostructures.

Fig. 6 (a) Kinetic relationship between removal efficiency and adsorption time; and (b) the corresponding pseudo-second-order models of the kinetic processes.

Fig. 7 (a) Adsorption isotherms of the snowflake-shaped ZnO@SiO₂@Fe₃O₄/C adsorbents towards: Pb(II), As(V) and MB (the lines stand for the results from Langmuir adsorption model fits); (b) the linearized fits based on Langmuir adsorption model.

Fig. 8 (a) The removal efficiency of the snowflake-shaped ZnO@SiO₂@Fe₃O₄/C adsorbents under different pH values; (b) the removal efficiency of the adsorbents towards Pb(II) in three cycling procedures.

Table 1 Comparison on the maximum adsorption capacities (unit: mg g⁻¹) between the presented snowflake-shaped adsorbents with some other reports.



Scheme 1 The illustration for the fabrication of a snowflake-shaped magnetic adsorbent.

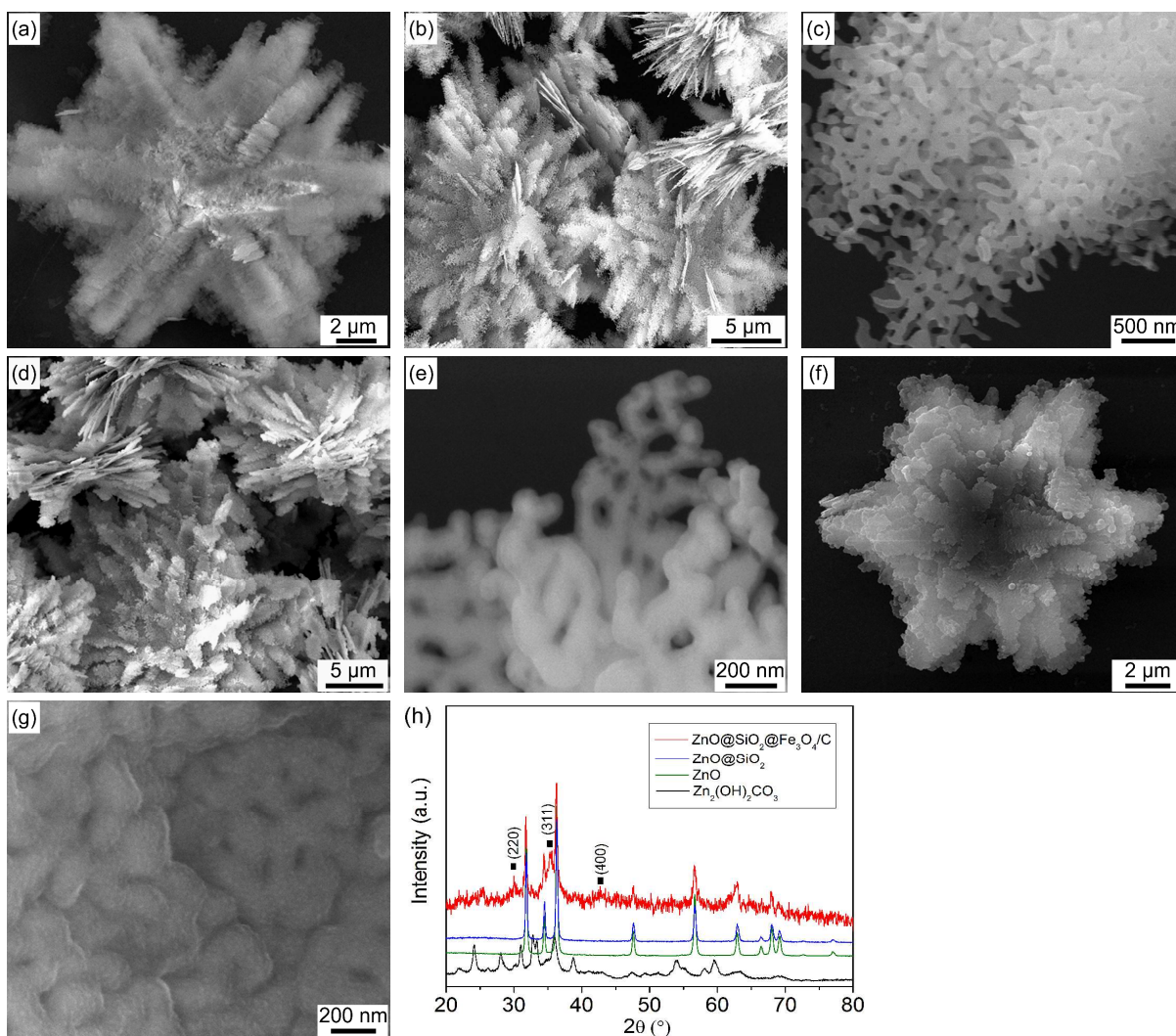


Fig. 1 FESEM images of (a) the prepared precursors; (b) and (c) ZnO; (d) and (e) SiO₂-coated ZnO; (f) and (g) ZnO@SiO₂@Fe₃O₄/C micro-/nanostructures; and (h) XRD patterns of the samples.

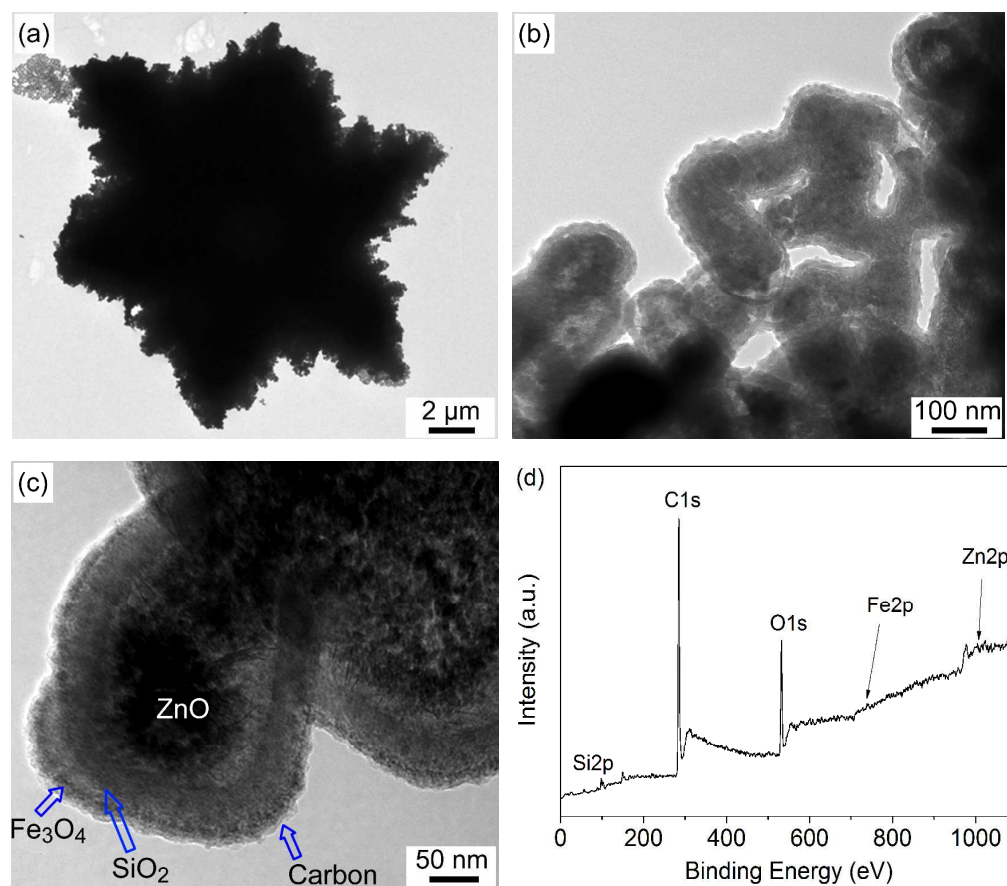


Fig. 2 TEM images of a single snowflake-shaped $\text{ZnO@SiO}_2\text{@Fe}_3\text{O}_4/\text{C}$; (b) and (c) high-magnification TEM images; and (d) XPS spectrum of the $\text{ZnO@SiO}_2\text{@Fe}_3\text{O}_4/\text{C}$ micro-/nanostructures.

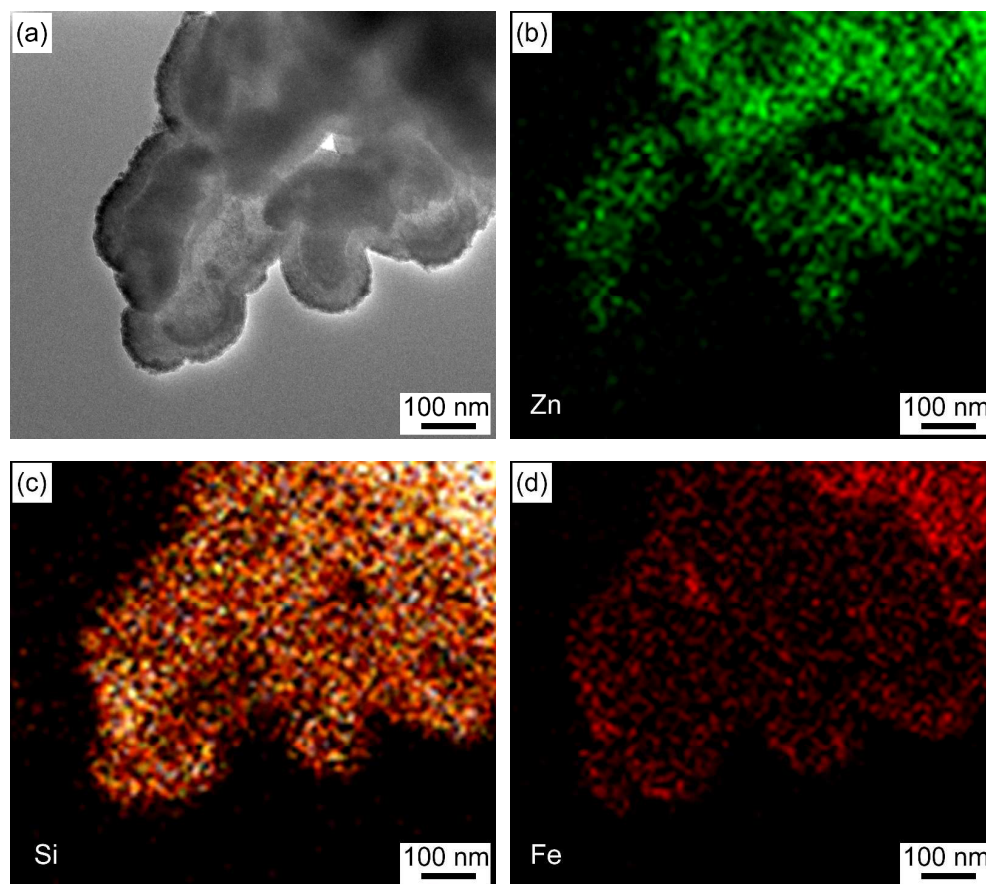


Fig. 3 High-magnification TEM image of a part of the snowflake-shaped ZnO@SiO₂@Fe₃O₄/C micro-/nanostructure; elemental mappings of (b) Zn K α , (c) Si K α , and (d) Fe K α .

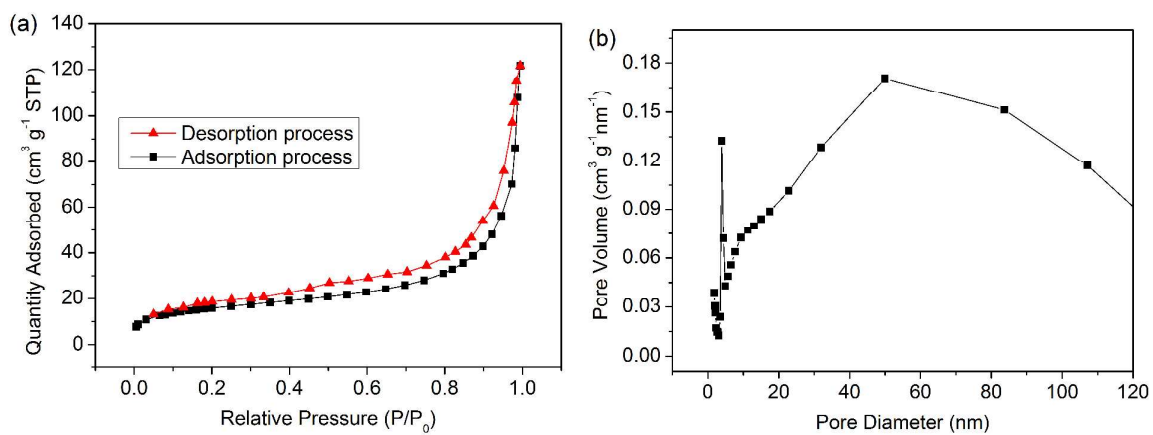


Fig. 4 (a) Typical N₂ adsorption/desorption isotherm and (b) pore-size distribution curve of the porous ZnO@SiO₂@Fe₃O₄/C micro-/nanostructure.

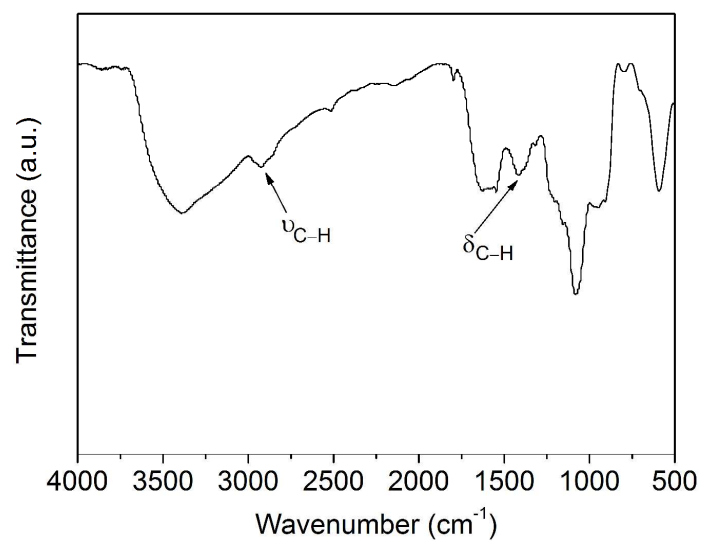


Fig. 5 FTIR spectrum of the snowflake-shaped ZnO@SiO₂@Fe₃O₄/C micro-/nanostructures.

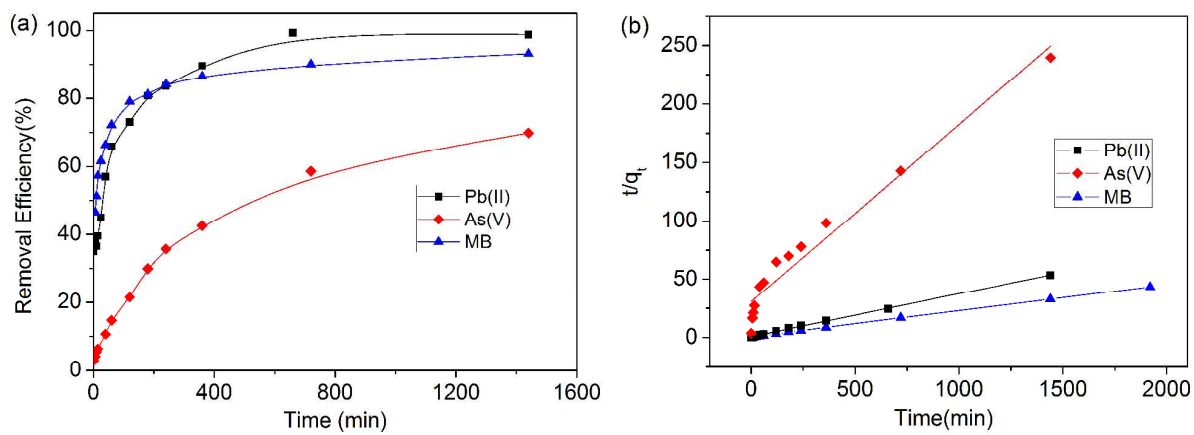


Fig. 6 (a) Kinetic relationship between removal efficiency and adsorption time; and (b) the corresponding pseudo-second-order models of the kinetic processes.

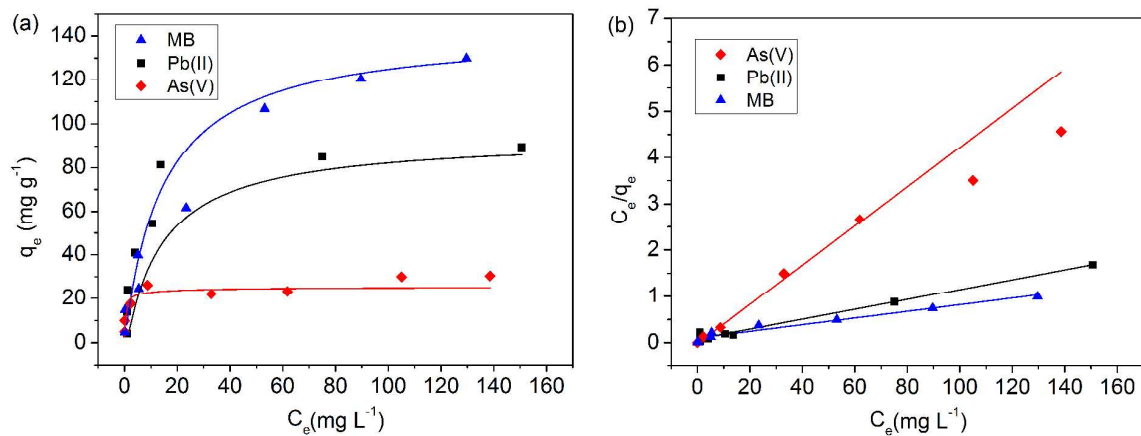


Fig. 7 (a) Adsorption isotherms of the snowflake-shaped ZnO@SiO₂@Fe₃O₄/C adsorbents towards: Pb(II), As(V) and MB (the lines stand for the results fitted from Langmuir isotherm model); (b) the linearized fits based on Langmuir adsorption model.

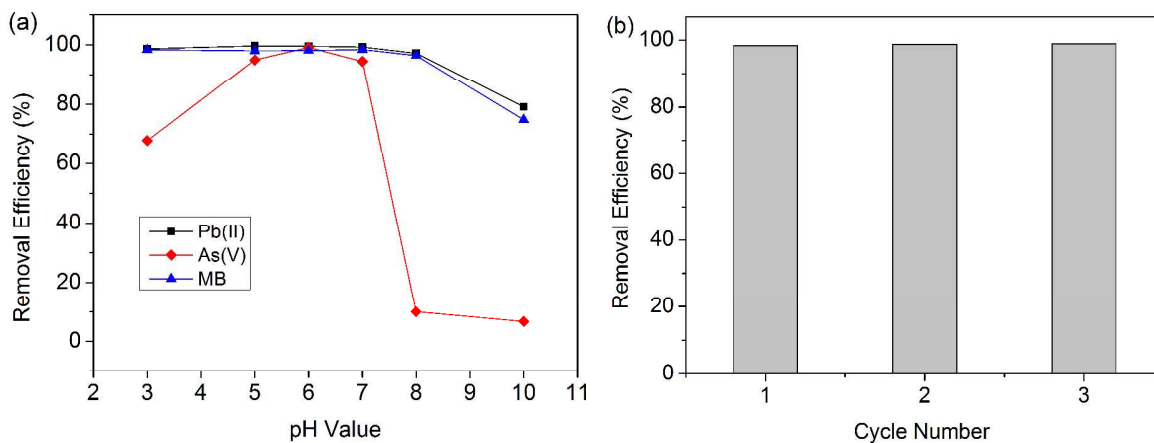


Fig. 8 (a) The removal efficiency of the snowflake-shaped ZnO@SiO₂@Fe₃O₄/C adsorbents under different pH values; (b) the removal efficiency of the adsorbents towards Pb(II) in three cycling procedures.

Table 1 Comparison on the maximum adsorption capacities (unit: mg g^{-1}) between the presented snowflake-shaped adsorbents with some other reports.

Adsorbents	Pb(II)	As(V)	MB	Ref.
magnetic $\text{Fe}_3\text{O}_4@/\text{SiO}_2$ ion-imprinted polymer	32.6	-	-	45
dithiooxamide-functionalized chelating resin	24.3	-	-	46
Polystyrene-EDTA resin	32.1	-	-	47
flower-like hierarchical iron oxides	-	5.3	-	48
superparamagnetic acid-coated Fe_3O_4 nanoparticles	-	16.6	-	49
graphene oxide	-	-	17.3	50
magnetite@graphene	-	-	45.3	51
silver nanoparticles loaded on activated carbon	-	-	71.4	52
snowflake-shaped $\text{ZnO}@/\text{SiO}_2@/\text{Fe}_3\text{O}_4/\text{C}$	94.3	23.6	142.9	in our study

References

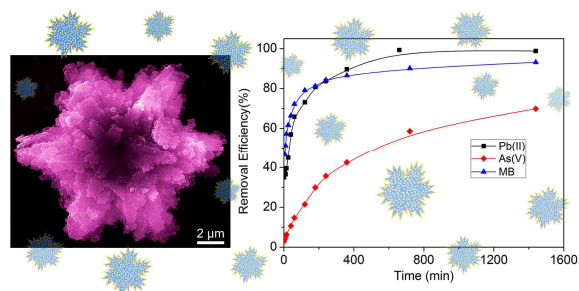
- 1 T. M. Clancy, K. F. Hayes and L. Raskin, *Environ. Sci. Technol.*, 2013, **47**, 10799–10812.
- 2 S. C.N. Tang and I. M.C. Lo, *Water Res.*, 2013, **47**, 2613–2632.
- 3 Z. Y. Cai, Z. G. Xiong, X. M. Lu and J. H. Teng, *J. Mater. Chem. A*, 2014, **2**, 545–553.
- 4 P. Dhiman, J. Chand, A. Kumar, R. K. Kotnala, K. M. Batoo and M. Singh, *J. Alloys Compd.*, 2013, **578**, 235–241.
- 5 Y. L. Min, G. Q. He, Q. J. Xu and Y. C. Chen, *J. Mater. Chem. A*, 2014, **2**, 1294–1301.
- 6 R. L. Babu, E. Vijayalakshmi, M. N. Kumar, R. H. Patil, K. S. Devaraju and S. C. Sharma, *Biorem. J.*, 2013, **17**, 231–239.
- 7 J. Singh and A. S. Kalamdhad, *Environ. Sci. Pollut. Res.*, 2013, **20**, 8974–8985.
- 8 F. Yu, L. Chen, J. Ma, Y. R. Sun, Q. Li, C. L. Li, M. X. Yang and J. H. Chen, *RSC Adv.*, 2014, **4**, 5518–5523.
- 9 Y. M. Zhang, Z. A. Qiao, Y. T. Li, Y. L. Liu and Q. S. Huo, *J. Mater. Chem.*, 2011, **21**, 17283–17289.
- 10 H. C. Gao, Y. M. Sun, J. J. Zhou, R. Xu and H. W. Duan, *ACS Appl. Mater. Interfaces*, 2013, **5**, 425–432.
- 11 N. M. Mubarak, J. N. Sahu, E. C. Abdullah and N. S. Jayakumar, *Sep. Purif. Rev.*, 2014, **43**, 311–338.
- 12 L. H. Velazquez-Jimenez, R. H. Hurt, J. Matos and J. R. Rangel-Mendez, *Environ. Sci. Technol.*, 2014, **48**, 1166–1174.
- 13 Q. Du, S. J. Zhang, B. C. Pan, L. Lv, W. M. Zhang and Q. X. Zhang, *Water Res.*, 2013, **47**, 6064–6074.

- 14 S. Wang, Y. Y. Zhai, Q. Gao, W. J. Luo, H. Xia and C. G. Zhou, *J. Chem. Eng. Data*, 2014, **59**, 39–51.
- 15 Y. R. Zhang, D. J. Liang, M. Wu, X. H. Zhao and X. J. Yang, *Chin. J. Inorg. Chem.*, 2013, **29**, 628–634.
- 16 S. B. Yang, D. D. Shao, X. K. Wang and M. Nagatsu, *RSC Adv.*, 2014, **4**, 4856–4863.
- 17 W. Gao, X. M. Feng, A. Pei, C. R. Kane, R. Tam, C. Hennessy and J. Wang, *Nano Lett.*, 2014, **14**, 305–310.
- 18 Y. M. Zheng, H. Bai, Z. B. Huang, X. L. Tian, F. Q. Nie, Y. Zhao, J. Zhai and L. Jiang, *Nature*, 2010, **463**, 640–643.
- 19 Z. W. Wang, L. Q. Zhu, W. P. Li and H. C. Liu, *ACS Appl. Mater. Interfaces*, 2013, **5**, 10904–10911.
- 20 J. Y. Liu, T. Luo, S. T. Mouli, F. L. Meng, B. Sun, M. Q. Li and J. H. Liu, *Chem. Commun.*, 2010, **46**, 472–474.
- 21 X. Q. Fu, J. Y. Liu, Y. T. Wan, X. M. Zhang, F. L. Meng and J. H. Liu, *J. Mater. Chem.*, 2012, **22**, 17782–17791.
- 22 Y. T. Wan, J. Y. Liu, W. Li, F. L. Meng, Z. Jin, X. Y. Yu, X. J. Huang and J. H. Liu, *Nanotechnology*, 2011, **22**, 315501.
- 23 Q. Jing, W. Y. Fu, W. C. Li, H. B. Yang, M. H. Li, J. W. Ma, X. M. Zhou, M. L. Sun, H. Zhao, Y. Y. Zhang, W. Y. Zhao, L. N. Zhang and H. Chen, *Appl. Surf. Sci.*, 2012, **258**, 3604–3610.
- 24 J. Y. Liu, Z. Guo, F. L. Meng, T. Luo, M. Q. Li and J. H. Liu, *Nanotechnology*, 2009, **20**, 125501.
- 25 H. C. Zeng and S. K. Tung, *Chem. Mater.*, 1996, **8**, 2667–2672.

- 26 N. M. Mubarak, J. N. Sahu, E. C. Abdullah and N. S. Jayakumar, *Sep. Purif. Rev.*, 2014, **43**, 311–338.
- 27 H. B. Liu, T. H. Chen, J. Chang, X. H. Zou and R. L. Frost, *J. Colloid Interface Sci.*, 2013, **398**, 88–94.
- 28 H. J. Oh, H. R. Jang, K. Y. Jung and J. H. Kim, *Microporous Mesoporous Mater.*, 2013, **180**, 109–113.
- 29 J. L. Mohanan, I. U. Arachchige and S. L. Brock, *Science*, 2005, **307**, 397–400.
- 30 S. Grosshans-Vieles, F. Tihay-Schweyer, P. Rabu, J. L. Paillaud, P. Braunstein, B. Lebeau, C. Estournes, J. L. Guille and J. M. Rueff, *Microporous Mesoporous Mater.*, 2007, **106**, 17–27.
- 31 R. K. Rana, L. Z. Zhang, J. C. Yu, Y. Mastai and A. Gedanken, *Langmuir*, 2003, **19**, 5904–5911.
- 32 Y. Huang, S. X. Li, J. H. Chen, X. L. Zhang and Y. P. Chen. *Appl. Surf. Sci.*, 2014, **293**, 160–168.
- 33 S. Kant, D. Pathania, P. Singh, P. Dhiman and A. Kumar. *Appl. Catal. B*, 2014, **147**, 340–352.
- 34 B. E. Reed, R. Vaughan and L. Q. Jiang, *J. Environ. Eng.*, 2000, **126**, 869–873.
- 35 V. P. Vinod and T. S. Anirudhan, *Water Air Soil Poll.*, 2003, **150**, 193–217.
- 36 E. E. Ozbas, A. Ongen and C. E. Gokce, *Desalination Water Treat.*, 2013, **51**, 7523–7535.
- 37 Y. G. Peng, D. J. Chen, J. L. Ji, Y. Kong, H. X. Wan and C. Yao, *Environ. Prog. Sustainable Energ.*, 2013, **32**, 1090–1095.
- 38 S. Chegrouche, A. Mellah and S. Telmoune, *Water Res.*, 1997, **31**, 1733–1737.
- 39 M. T. Ghaneian, G. Ghanizadeh, M. T. H. Alizadeh, M. H. Ehrampoush and F. M. Said, *Environ. Technol.*, 2014, **35**, 882–890.
- 40 X. W. Zhao, Q. Jia, N. Z. Song, W. H. Zhou and Y. S. Li, *J. Chem. Eng. Data*, 2010, **55**,

- 4428–4433.
- 41 M. Naushad, *Chem. Eng. J.*, 2014, **235**, 100–108.
- 42 T. T. Sheng, S. A. Baig, Y. J. Hu, X. Q. Xue and X. H. Xu, *Arabian J. Chem.*, 2014, **7**, 27–36.
- 43 P. Fei, M. Zhong, Z. Q. Lei and B. T. Su, *Mater. Lett.*, 2013, **108**, 72–74.
- 44 C. N. Delgado and J. R. R. Mendez, *Water Res.*, 2012, **46**, 2973–2982.
- 45 B. Guo, F. Deng, Y. Zhao, X. B. Luo, S. L. Luo and C. T. Au, *Appl. Surf. Sci.*, 2014, **292**, 438–446.
- 46 S. Dutta and A. K. Das, *J. Appl. Polym. Sci.*, 2007, **103**, 2281–2285.
- 47 L. Y. Wang, L. Q. Yang, Y. F. Li, Y. Zhang, X. J. Ma and Z. F. Ye, *Chem. Eng. J.*, 2010, **163**, 364–372.
- 48 J. S. Hu, L. S. Zhong, W. G. Song and L. J. Wan, *Adv. Mater.*, 2008, **20**, 2977–2982.
- 49 L. Feng, M. Cao, X. Ma, Y. Zhu and C. Hu, *J. Hazard. Mater.*, 2012, **217**, 439–446.
- 50 G. K. Ramesha, A. V. Kumara, H. B. Muralidhara and S. Sampath, *J. Colloid Interface Sci.*, 2011, **361**, 270–277.
- 51 Y. Yao, S. Miao, S. Liu, L. P. Ma, H. Sun and S. Wang, *Chem. Eng. J.*, 2012, **184**, 326–332.
- 52 M. Ghaedi, S. Heidarpour, S. N. Kokhdan, R. Sahraie, A. Daneshfar and B. Brazesh, *Powder Technol.*, 2012, **228**, 18–25.
- 53 Z. Y. Zhang and J. L. Kong, *J. Hazard. Mater.*, 2011, **193**, 325–329.
- 54 R. H. Wu, J. H. Liu, L. Q. Zhao, X. L. Zhang, J. R. Xie, B. W. Yu, X. L. Ma, S. T. Yang, H. F. Wang and Y. F. Liu, *J. Environ. Chem. Eng.*, 2014, **2**, 907–913.

Table of contents entry



A novel snowflake-shaped micro-/nanoparticle was reported as a highly-efficient adsorbent for removing pollutants from aqueous solution.